International Communications in Heat and Mass Transfer 98 (2018) 304–309

Contents lists available at ScienceDirect

International Communications in Heat and Mass Transfer

journal homepage: www.elsevier.com/locate/ichmt

Molecular Dynamic Simulations of Fibrous Distillation Membranes

A.A. Hemeda[a,b], R.J.A. Esteves[b], J.T. McLeskey Jr[b], M. Gad-el-Hak[a], M. Khraisheh[c], H. Vahedi Tafreshi[a,*]

[a] Department of Mechanical and Nuclear Engineering, Virginia Commonwealth University, Richmond, Virginia 23284, USA
[b] Department of Physics, Randolph-Macon College, Ashland, Virginia 23005, USA
[c] Department of Chemical Engineering, Qatar University, Doha, Qatar

ARTICLE INFO

Keywords:
Membrane distillation
Hydrophobicity
Desalination
Molecular dynamics simulation
Porous media
Mass transfer

ABSTRACT

The rate of heat and mass transfer through distillation membranes is typically estimated using an over-simplified, straight-cylindrical-pore approach coupled with several empirical correction factors that are included to compensate for the simplicity of the approach. In the present work, we have calculated for the first time the rate of transport of heat and mass through three-dimensional virtual membranes from first principles without the need for any empirical correction factors. More specifically, molecular dynamic (MD) simulations are conducted in idealized 3-D geometries that resemble the microstructure of a nanofiber membrane. The SPC/E molecular model and coarse-grain Pea model are considered to simulate, respectively, water molecules and air. The fibers, on the other hand, are constructed as simple metal lattice, and their contact angle with water is controlled using a scaling factor from the Lorentz–Berthelot mixing parameters. A proof-of-concept study is presented to demonstrate the capabilities of the new modeling approach in predicting the effects of the membrane's microstructural properties on the desalination performance. While the simulations are conducted at scales 3–4 orders of magnitudes smaller than an actual electrospun membrane, the conclusions can be applied membranes with more practical dimensions.

1. Introduction

Scarcity of fresh water is a major global concern that is expected to worsen as the impact of global warming on our planet becomes more severe in the next decades. When a modest amount of energy is available, direct-contact membrane distillation (DCMD) is a method for producing freshwater by creating a temperature difference between the feed (warm salty water) and permeate (cold purified water) separated from one another by a hydrophobic membrane [1,2]. The temperature difference across the membrane, in turn, creates a vapor pressure gradient that serves as the driving mechanism for the transport of water vapor from the feed to the permeate through the pores of the membrane (see Fig. 1). Mass transfer through a DCMD membrane is directly related to fresh water production rate and should be maximized, while heat transfer should be minimized to maintain a temperature difference across the membrane [3]. Therefore, developing computational tools that allow one to predict the rate of heat and mass transport through a DCMD membrane can be very beneficial in optimizing the microstructure of such membranes.

Vapor transport through a membrane can generally be characterized using the concept of molecular diffusion through a straight cylindrical pore [1–8]. Such a model can be incorporated in a larger (continuum flow) numerical simulation that includes the feed and permeate flow and temperature fields outside the membrane [1,9–13]. This classical approach relies on predetermined empirical factors/relationships that compensate for the over-simplified description of the membrane's microstructure. Being empirical in nature, those correction factors can only be used in studying the particular membrane for which they were obtained [14].

To overcome the aforementioned limitations, the present study is devised to investigate how molecular dynamic simulations (MD) can be used to simulate vapor transport through a DCMD membrane without (or with minimal) use of case-dependent empirical factors. Creating a universally-applicable simulation method will allow for optimizing the microstructure of the membranes for different flow conditions. The present paper is, however, only a starting point in our path to this ambitious goal. The present research is in fact the first to consider MD simulations to predict the rate of mass and transfer through a DCMD membrane. Given the complicated internal porous structure of membranes produced via film extrusion, we have focused our study on

* Corresponding author.
E-mail address: htafreshi@vcu.edu (H. Vahedi Tafreshi).

https://doi.org/10.1016/j.icheatmasstransfer.2018.09.012

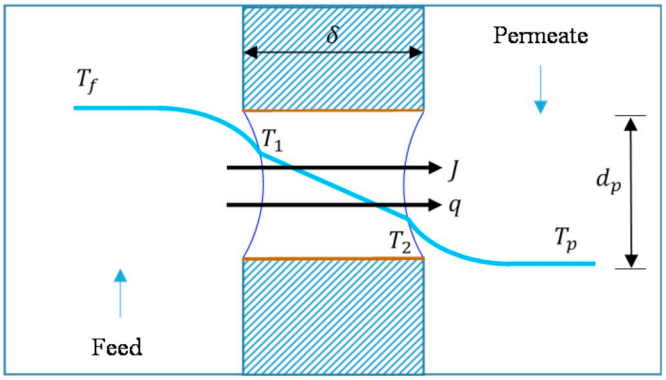

Fig. 1. Traditional approach to study distillation membranes where membrane pores are represented as a straight cylindrical hole with a length of δ and a diameter of d_p. The difference between the feed temperature T_f and permeate temperature T_p temperatures is the main driving force for vapor transport across the membrane.

membranes made of hydrophobic fibers (e.g., electrospun membranes [15,16]) known for their well-defined microstructures. While many membranes for DCMD are produced through solution-based electrospinning, there is a growing desire for using melt-electrospinning which provides a pathway for controlled fiber deposition [17,18]. Such controlled fiber deposition allows for predetermined pore geometry and uniformity compared to the random nature of solution electrospinning [15–18]. For the sake of simplicity, the virtual membranes are made of orthogonally-oriented fibers as might be prepared through melt-electrospinning methods. The fiber orientation in this study was kept constant while variables such as fiber diameter, hydrophobicity, and spacing were explored.

In the remainder of this paper, we first describe our approach toward MD simulations in Section 2, and then present a case where MD simulations are used to model vapor transport in a simplified virtual membrane in Section 3. The conclusions drawn from our study are given in Section 4.

2. Molecular Dynamic Simulations

MD is a molecular-level simulation approach based on integrating the equations of motion written for every atom in a substance over time [19]. The initial position and velocity of these atoms are used as the starting conditions in the integration process to predict future positions and velocities for the entire system [19–22]. In this work, the equations of motion are integrated using the Velocity–Verlet algorithm [23]. Using the principles of statistical mechanics, system properties (e.g., energy, temperature, and pressure) are then quantified and reported. The interaction between the molecules in an MD simulation is presented in terms of interatomic (bonded or non-bonded) potential energy [24]. The LAMMPS MD simulation code is used in our study for its flexibility and proven accuracy [25,26]. Certain assumptions have been considered to help speed up the otherwise computer-intensive MD calculations, as will be discussed later in this section.

An SPC/E water model is considered to model the interactions between water molecules [27,28]. The SPC model is proven to provide fairly accurate predictions for physical properties such as density, surface tension, and heat of evaporation, in good agreement with experimental results [27,28]. In this model, the total potential energy $U_{ij}^{SPC/E}$ of an interacting pair of particles i and j is.

$$U_{ij}^{\mathrm{SPC/E}} = U_{ij}^{\mathrm{disp}} + U_{ij}^{\mathrm{LRC}} + U_{ij}^{\mathrm{Coulomb}} \quad (1)$$

where the superscripts “disp”, “LRC”, and “Coulomb” stand for pair dispersion energy, long-range correction to the pair dispersion energy, and the Coulombic potential energy, respectively [25,26,28–30].

The traditional Lennard-Jones (LJ) intermolecular potential energy is considered for the pair dispersion energy [26]. The term U_{ij}^{LRC} is known as the long-range Coulombic potential which is calculated in the present work using the particle–particle particle–mesh (PPPM) method with an accuracy of 1×10^{-4} [30].

Since the long-range interaction of the Coulombic term is highly important for the surface tension calculations of the SPC/E model, an Ewald sum is introduced to correct these interactions [25,29–33]. Moreover, for the LJ term, an empirical tail correction is introduced to recover the discrepancies caused by these long-term interactions in the Coulombic term [31–33]. The SHAKE algorithm is utilized to constrain the internal geometry of each water molecule with time [25]. In the flexible isosceles triangle model of SPC/E model, constant charges of −0.8476 e and 0.4238 e were considered for the oxygen and hydrogen atoms, respectively. For the intramolecular bonds in the SPC/E model, the harmonic bond was assumed to be $\frac{1}{2}k_b(r - r_0)^2$ with an amplitude of $k_b = 1000.0$ eV/A^2 and distance-parameter of $r_0 = 1.0$ A, while the angle bond can be written as $\frac{1}{2}k_\theta(\theta - \theta_0)^2$ with an amplitude of $k_\theta = 1000.0$ eV and angular-parameter of $\theta_0 = 109.47^{\circ}$ [34]. The open-source code of LAMMPS is used for the modeling of these bonds [26].

To examine the accuracy of the SPC/E model, we compared its predictions against those obtained from the TIP4P model (a four-site molecule), which is a more accurate water molecule model (but computationally much slower). We simulated a water droplet with an arbitrary diameter and temperature using both the SPC/E and TIP4P models with identical initial input parameters. Using the Laplace equation, surface tension values of 0.0635 N/m and 0.0748 N/m at $T = 300$ K were obtained from, respectively, the SPC/E and TIP4P simulations. From SPC/E there is an underestimation of about 12% in the surface tension compared to the experimental value of 0.072 N/m [35]. This is because the SPC/E model is non-polarizable [36], and there is also an overestimation of the diffusion constant where the hydrogen bonding is not sufficiently simulated in the SPC/E model [20,37].

The smallest computational domain considered for the simulations reported here is shown in Fig. 2 (larger domains are created by repeating the 4-fiber unit cell shown in the figure in the z-direction). To

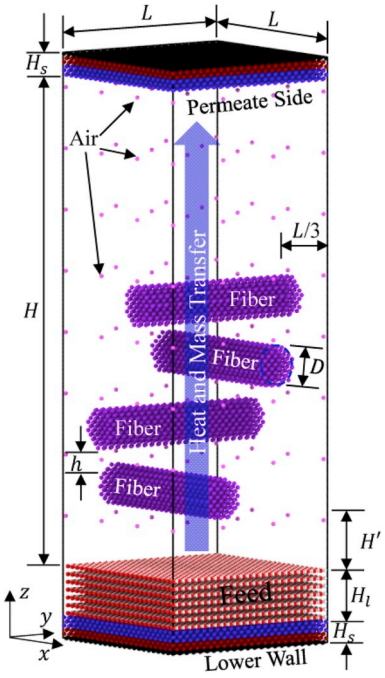

Fig. 2. Smallest simulation domain (unit cell) comprised of four fibers between two parallel boundaries with spacing H. Larger domains are created by repeating the 4-fiber unit cell in the z-direction.

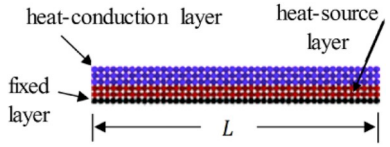

Fig. 3. Three sets of layers (fixed, heat-source, and heat conducting layers) used to represent the feed and permeate walls in the computational domain.

simplify the challenging task of modeling heat and mass transfer through a membrane with discorded fibrous microstructures, our virtual membranes are assumed to be comprised of orthogonally-oriented layers of parallel fibers. The domain is a square-ended box with side length L and height H. The fibers are distributed vertically in contact with each other with a distance of $H^{'}$ between the water and the fiber boundary, as shown in Fig. 2. A film of water (i.e., red and white atoms representing, respectively, the oxygen and hydrogen atoms in the water molecule) with a given thickness H_l is placed on top of the bottom wall. Each fiber (purple atoms) is assumed to be a cylinder with a diameter of D.

The first design parameter of a fibrous membrane is the solid volume fraction (SVF) defined as,

$$\phi = \frac{\pi D^2}{LH} \quad (2)$$

To minimize the number of atoms required to model the polymeric fibers (made of large-chain molecules), we assumed the fibers to be made of copper. This simplification significantly reduced the required CPU time. Each fiber consists of a fixed (frozen atoms) inner layer to maintain the cylindrical shape and spatial location of the fiber. The copper is assumed to be a faced-center cube (FCC) system with a lattice length of 3.62 Å for a density of 8.9 g/cm3. Also, the distance and energy parameters of LJ are assumed to be 2.34 Å and 0.4095 eV, respectively [38,39]. The copper fibers are set to mimic the hydrophobic behavior of polymeric fibers by controlling their contact angle using a parameter r as will be discussed later [40–42].

The solid walls are comprised of six atomic layers made of copper [39,43,44]. The first bottom-layer is fixed to act as a boundary for the computational domain as shown in Fig. 3 with black atoms. The next two layers are designated as a heat source (or sink) to the system using a Langevin thermostat (red atoms in Fig. 3) [38,39,43]. In the Langevin mathematical approach, a set of stochastic differential equations is carried out to maintain the system temperature in molecular dynamic simulations [43,44]. The last three top layers (blue atoms) are designated as heat-conduction layers to transfer the heat to water, i.e., heat up (feed side) or cool down (permeate side) the water film in contact with the wall. Note that for the wall on the permeate side, the layer construction is mirrored in order to bound the computational domain from upper side. This approach allows for good control over the system's temperature and has been adapted from previous studies [38,39,43].

For simplicity, we assume the air to be made only of nitrogen as the molecular weight of air is almost the same as that of bi-atomic nitrogen gas, and it is simulated using a coarse-grain (Pea) model [45,46]. The air is shown in Fig. 2 in light-violet color while the solid wall particles are shown in the dark-violet.

The parameters of the LJ potential equation for the interactions between two different molecules (e.g., water and solid wall or fiber) are calculated based on Lorentz–Berthelot mixing rules [47,48]. The

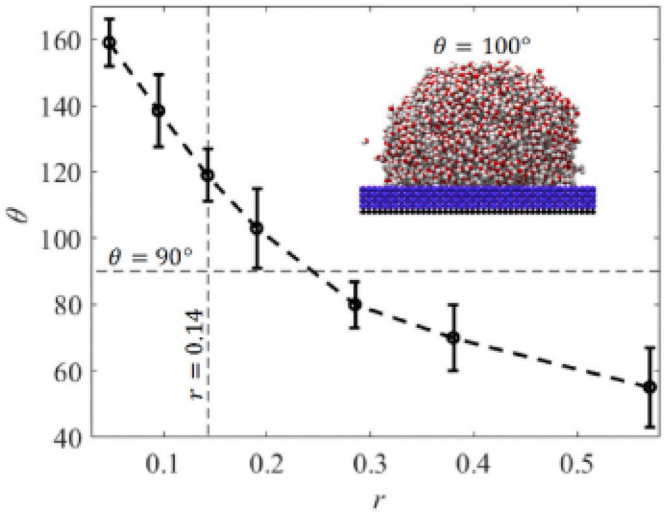

Fig. 4. Effects of the r-factor on droplet contact angle on a flat surface. Inset shows a snapshot in time of a droplet on surface with $r = 0.14$ corresponding to an expected average contact angle of about 90°.

distance parameter σ_{ij} is calculated as an arithmetic mean.

$$\sigma_{ij} = \frac{1}{2}(\sigma_i + \sigma_j) \quad (3)$$

where the subscripts i and j represent the two interacting molecules. The standard energy term in the LJ potential equation is given as a geometric mean.

$$\epsilon_{ij} = r\sqrt{\epsilon_i \epsilon_j} \quad (4)$$

where the factor r is used to change the surface wettability with water (e.g., for $r < < 1$, the surface is superhydrophobic). We used the factor r in the original Lorentz–Berthelot mixing rules to change the surface wettability of the fibers [47]. For instance, an r-factor of $r = 0.024$ represents a Young–Laplace contact angle (YLCA) of about 90°. Note that Eqs. (3) and (4) are used for interactions between all other atom pairs with $r = 1$ such as nitrogen (atom i) and solid walls (atom j), or nitrogen (atom i) and water atoms (molecule j), and vice versa. In the present work, a potential cut-off radius of 2.5 Å is used, and $\epsilon = 0.00675$ eV and $\sigma = 3.167$ Å are the standard energy and distance used in the SPC/E model [28].

Fig. 4 shows a water droplet consisting of 4096 water molecules on a flat surface. For this simulation, the initial droplet shape was assumed to be cubic, and the initial velocity was calculated based on a Gaussian distribution for the solid wall and water particles at room temperature. The factor r is varied from 0.004 to 1.0 to simulate surfaces with different YLCAs. It is readily seen that the factor r can be used to adjust the wettability of the fibers.

3. Results and Discussions

In this section, we present the results of the MD simulations obtained for a virtual DCMD system operating under different operating conditions and geometric parameters. We start first by using a test case as a reference. The effects of several parameters on the mass flux are then calculated.

In the test (or reference) case, the domain dimensions are chosen to be $L = 82$ Å, $H^{'} = 35$ Å, $H_l = 20$ Å, and $D = 18$ Å, with a solid volume fraction (SVF) of $\phi = 0.063$. The fibers are assumed to be in contact

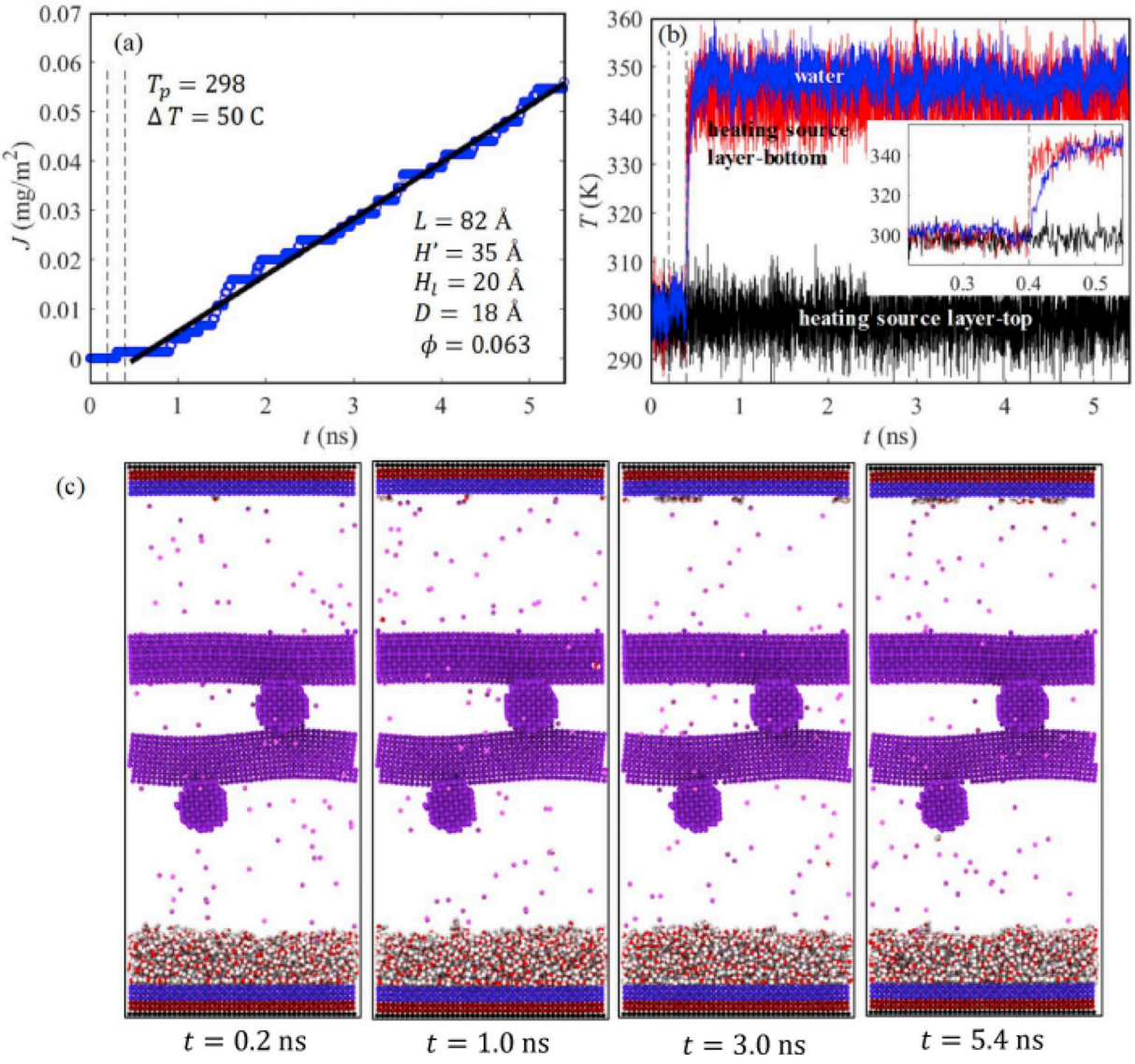

Fig. 5. Case study with a solid volume fraction of 0.063, $L = 82$ Å, $H^{'} = 35$ Å, $H_l = 20$ Å, $\Delta T = 50^{\circ}$C, and $T_p = 298^{\circ}$C. (a) Mass transfer per unit area across the membrane, slope represents the flux s kg/m^2.s. (b) Transient temperature of water and top and bottom layers. (c) Snapshots of vapor transport through membrane at different times between 0 and 5.4 ns.

with each other, i.e., $h = 0.0$. The time step and r-factor were set as, respectively, 1.0 fs and 0.14 (i.e., contact angle of 90°), respectively. A feed and permeate temperatures of, respectively, 348 K and 298 K were chosen.

The simulations started with an initial temperature of 298 K. The NVE ensemble (defined as a microcanonical ensemble with constant number of particles N, system volume V, and system energy E) along with Langevin thermostats were used for a short initialization stage of $0 < t < 200$ ps. The thermostats were then all switched off, except for the heating source layers of the lower and upper walls, and the system was allowed to equilibrate for another 200 ps (equilibrium stage). The purpose of this stage was to ensure that there was no increase in the system temperature while a constant energy ensemble was running (Fig. 5a and b). Next, the temperature of the heating layers in the lower walls (feed) was rapidly increased to 348 K using the Langevin thermostat while the temperature of the heating source layer (permeate) at the top remained at 298 K, as shown in Fig. 5b.

Note that an NVE ensemble was used in the rest of the computational domain without a thermostat. Fig. 5a shows the vapor mass transport across the membrane versus time for the first 5 ns of the simulations. As can be seen, the mass transfer is almost linear with time with a slope (i.e., mass flux) of about $s = 0.012$ kg/m^{2}s. Fig. 5c shows snapshots from the simulations at different times.

Fig. 6 is prepared to discuss the effects SVF on the mass flux through the membrane. Note that SVF can be varied by varying fiber diameter when the width of the simulation domain is kept constant (Fig. 6a) or

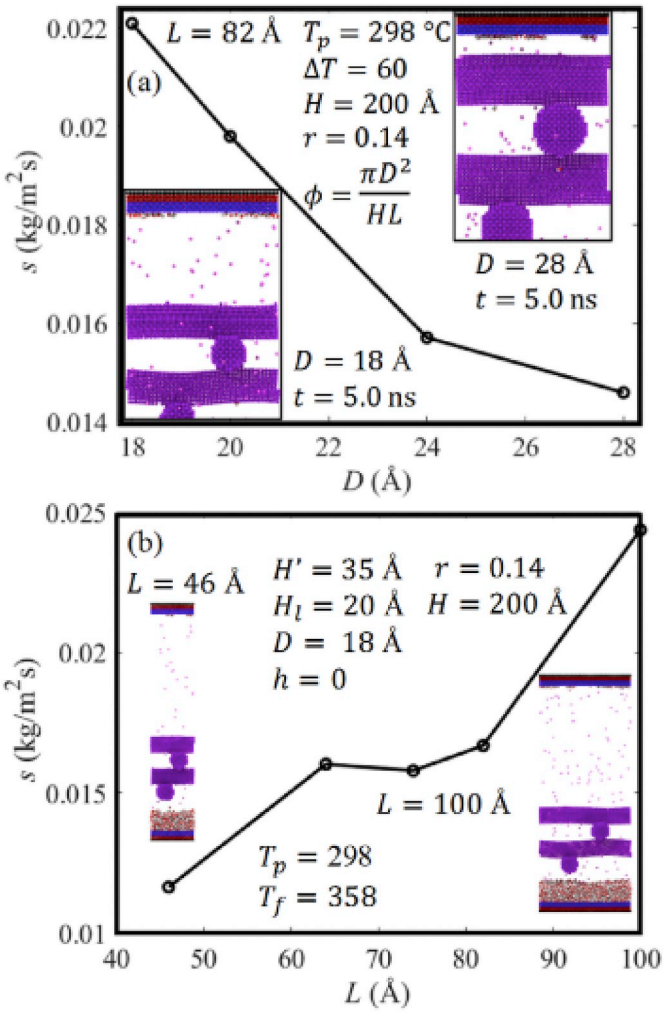

Fig. 6. Effects varying membrane's solid volume fraction by varying fiber diameter in a computational domain with fixed dimensions (a) or by varying the size of the computational domain when fiber diameter is kept constant (b). The inset images show membranes with different fiber diameters of in domains with different dimensions.

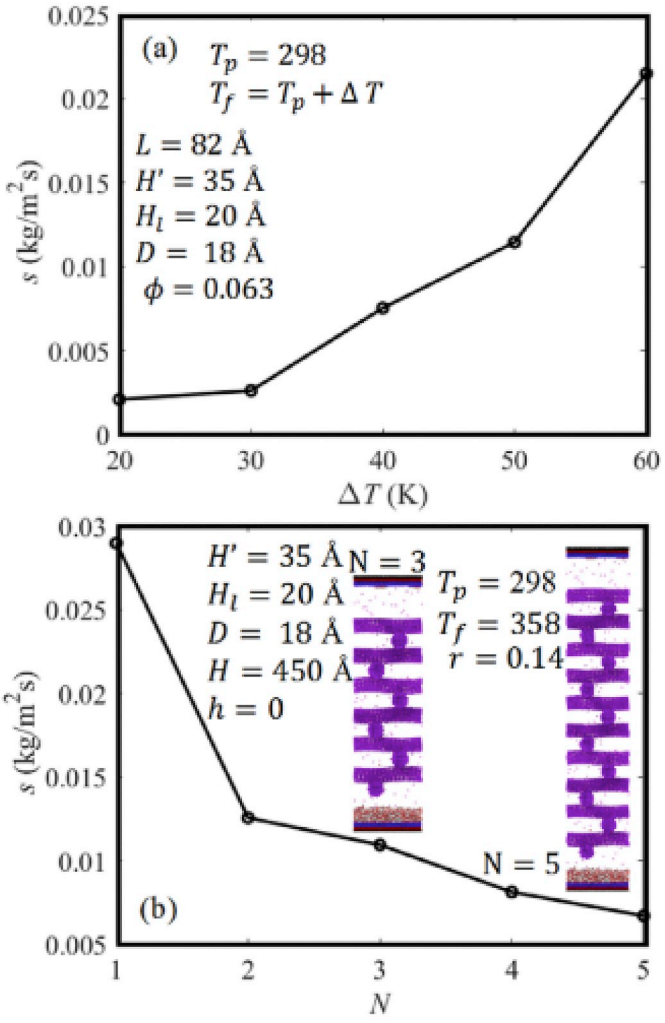

Fig. 7. Effects of temperature gradient (a) and membrane thickness (b) on the rate of mass transfer.

by varying width for a fixed fiber diameter (Fig. 6b). As can be seen in Fig. 6a, increasing the SVF decreases the mass flux through the membrane, which is in qualitative agreement with the physics of Knudsen and continuum flows in DCMD [2,7]. Likewise, decreasing the SVF by increasing the width of simulation box increases the flux as expected (Fig. 6b).

Fig. 7a shows the effects of temperature difference across the membrane on the vapor flux *s*, for a permeate temperature of 298 K but for five different ΔTs ranging from 20 to 60 K (five different feed temperatures). In qualitative agreement with previous studies, it can be seen that the vapor flux increases with increasing the temperature gradient across the membrane [2,7]. Fig. 7b shows the effects of membrane thickness on flux. It can be seen that vapor flux decreases with increasing membrane thickness, as expected.

The results of the present investigation can be used to estimate or optimize the membrane's configurations necessary to enhance the mass flux. Also, the stability of the membrane and/or thresholds of the different parameters can be predicted for the designer's considerations.

4. Conclusions

The work reported here is a proof-of-concept molecular dynamics simulation aimed at predicting the rate of heat and mass transfer across a fibrous DCMD membrane for the first time. While limited in the number of atoms and the dimensions of the virtual membranes, our molecular dynamics simulations could reveal the effects of membranes' microstructure on their desalination performance without the need for empirical correction factors. More specifically, the effects of fiber diameter, membrane porosity, membrane thickness, and temperature gradient across the membrane are simulated. While the simulations reported here have been conducted at scales 3–4 orders of magnitudes smaller than actual electrospun membranes, they prove the feasibility of using molecular dynamics as a tool to engineer next generation of DCMD membranes from first principles rather than try-and-error.

Acknowledgements

This research was made possible by a grant from the Qatar National Research Fund under its National Priorities Research Program award number NPRP No: 8-270-2-106. Its contents are solely the responsibility of the authors and do not necessarily represent the official views of the Qatar National Research Fund.

References

[1] A. Alkhudhiri, N. Darwish, N. Hilal, Membrane distillation: A comprehensive review, Desalination 287 (2012) 2–18.
[2] J. Phattaranawik, R. Jiraratananon, A.G. Fane, J. Membr. Sci. 212 (2003) 177–193.
[3] R. Ullah, M. Khraisheh, R.J. Esteves, J.T. McLeskey Jr, M. Alghouti, M. Gad-El-Hak, H.V. Tafreshi, Energy efficiency of direct-contact membrane distillation, Desalination (2018) 56–67.
[4] M. Khayet, T. Matsuura, J.I. Mengual, M. Qtaishat, Design of novel direct-contact membrane distillation membranes, Desalination 192 (2006) 105–111.
[5] M. J. -G. Lee, T. W-S. Kim, J.I. J-S. Choi, M. N. Ghaffour, M. Y-D. Kim, Dynamic solar-powered multi-stage direct-contact membrane distillation system: Concept design, modeling and simulation, Water Re. 107 (2017) (47-5).
[6] A. Ali, J.-H. Tsai, K.-L. Tung, E. Drioli, F. Macedonio, Designing and optimization of continuous direct-contact membrane distillation process, Desalination 426 (2018) 97–107.
[7] E.K. Summers, H.A. Arafat, J.H. Lienhard, Energy efficiency comparison of single stage membrane distillation (MD) desalination cycles in different configuration, Desalination 290 (2012) 54–66.
[8] M.S. El-Bourawi, Z. Ding, R. Maa, M. Khayet. A framework for better understanding membrane distillation separation process. J. Membr. Sci285. (2006) 4–29.
[9] S. Srisurichan, R. Jiraratananon, A.G. Fane, Mass transfer mechanisms and transport resistances in direct-contact membrane distillation process, J. Membr. Sci. 277 (2006) 186–194.
[10] A. K. Abdel-Rahman. Modeling Temperature and Salt Concentration Distribution in Direct-contact Membrane Distillation. Journal of Engineering Sciences, Assiut University 36 5 (2008) 1167–1188.
[11] H. Chang, C.-D. Ho, J.-A. Hsu, Analysis of heat transfer coefficients in direct-contact membrane distillation modules using CFD simulation, J. Appl. Sci. Eng. 19 197206 (2016) 2.
[12] M. Ghadiri, S. Fakhiri, S, Shirazian, Modeling and CFD Simulation of Water Desalination Using Nanoporous Membrane Contactors. Ind. Eng. Chem. Res. 52 (2013) 3490–3498.
[13] H. Yu, X. Yang, R. Wang, A.G. Fane, Numerical simulation of heat and mass transfer in direct membrane distillation in a hollow fiber module with laminar flow, J. Membr. Sci. 384 (2001) 1–2 (107–116).
[14] W. Kast, C.R. Hohenthanner, Mass transfer within the gas phase porous media, Int. J. Heat Mass Trans. 43 (2000) 807.
[15] M. Essalhi, M. Khayet, Self-sustained webs of polyvinylidene fluoride electrospun nano-fibers: effects of polymer concentration and desalination by direct-contact membrane distillation, J. Membr. Sci. 454 (2014) 133–143.
[16] L.D. Tijing, J.-S. Choi, S. Lee, S.-H. Kim, H.K. Shon, Recent progress of membrane distillation using electrospun nanofibrous membrane, J. Membr. Sci. 453 (2014) 435–462.
[17] J.A. Prince, D. Rana, T. Matsuura, N. Ayyanar, T.S. Shanmugasundaram, G. Singh, Nanofiber based triple layer hydro-philic/ – phobic membrane – a solution for pore wetting in membrane distillation, Scientific Report 4 (2014) 6949.
[18] T.D. Brown, P.D. Dalton, D.W. Hutmacher, Direct Writing By Way of Melt Electrospinning, Adv. Mater. 23 (2011) 5651–5657.
[19] S. Cheng, J.B.Lechman.S.J. Pilmptoon, G.S. Grest, Evaporation of Lennard-Jones fluids, The journal of Chemistry Physics 134 (2011) 122.
[20] H. Liu, G. Cao, Effectiveness of the Young-Laplace equation at nanoscale, Sci. Rep. 6 (2016) 23936.
[21] L. Martínez, R. Andrade, E.G. Birgin, J.M. Martínez, PACKMOL: A package for building initial configurations for molecular dynamics simulations, J. Comput. Chem. 30 (13) (2009) 2157–2164.
[22] R. Ranganathan, S. Rokkam,, T. Desai, P. keblinki, P. Cross, R. Burnes. Modeling high-temperature diffusion of gases in micro and mesoporous amorphous carbon. J. Chem. Phys. 143 (2015) 084701.
[23] N. Bou-Rabee, Time Integrators for Molecular Dynamics, Entropy 16 (2014) 138–162.
[24] M.P. Allen, D.J. Tildesley, Computer Simulation of Liquids, 1st ed., Oxford Science Publications, Oxford, 1987.
[25] P.J. Veld, S.J. Plimpton, G.S. Grest, Accurate and efficient methods for modeling colloidal mixtures in an explicit solvent using molecular dynamics, Comp. Phys. Comm. 179 (2008) 320–329.
[26] http://lammps.sandia.gov/.
[27] H. J. C. Berensden, J.R. Grigera, T.P. Straatsma. The missing term in effective pair potentials. J. Phys. Chem91. (1987) 6268.
[28] S. Chatterjee, Pablo G. Deenedetti, F.H. Stillinger, R. Lynden-Bell, A computational investigation of thermodynamics, structure, dynamics and solvation behavior in modified water models, J. Chem. Phys. 128 (2008) 124511.
[29] P. Ewald, Die Berechnung optischer und elektrostatischer Gitterpotentiale, Ann. Phys. 369 (1921) 253.
[30] J.P. Ryckaert, G. Ciccotti, H.J.C. Berendsen, Numerical integration of the Cartesian equations of motion of a system with constraints: molecular dynamics of *n*-alkanes, J. Comp. Phys. 23 (1977) 327–341.
[31] J. Alejandre, D.J. Tildesley, G.A. Chapela, Molecular dynamics simulation of the orthobaric densities and surface tension of water, J. Chem. Phys. 102 (1995) 4574.
[32] B. Shi, S. Sinha, V.K. Dhir, Molecular dynamics simulation of the density and surface tension of water by particle-particle particle-mesh method, J. Chem. Phys. 124 (2006) 204715.
[33] D. Zahn, B. Schilling, S.M. Kast, Enhancement of the Wolf Damped Coulomb Potential: Static, Dynamic, and Dielectric Properties of Liquid Water from Molecular Simulation, J. Phys. Chem. B 106 (2002) 10725–10732.
[34] T.I. Mizan, P.E. Savage, R.M. Ziff, Molecular Dynamics of Supercritical Water Using a Flexible SPC Model, J. Phys. Chem. 98 (1994) 13067–13076.
[35] K.A. Sharp, Water: Structure and Properties, Encyclopedia of Life Sciences, John Wiley & Sons, Ltd, 2001.
[36] J.T. Rivera, F.W. Starr, P. Paricaud, P.T. Cummings, Polarizable contributions to the surface tension of liquid water, J. Chem. Phys. 125 (2006).
[37] R. Chitra, P.E. Smith, A comparison of the properties of 2,2,2-trifluoroethanol and 2,2,2-trifluoroethanol/water mixtures using different force fields, J. Chem. Phys. 115 (2001) 5521–5530.
[38] H. R. Seyf, Y. Zhang. Molecular Dynamics Simulation of Normal and Explosive Boiling on Nanostructured Surface. J. Heat Transf. 135 (2013) 121503–1.
[39] Y. Mao, Y. Zhang, Molecular dynamics simulation on rapid boiling of water on a hot copper plate, Applied Theremail Engineering 62 (2) (2014) 607–612.
[40] J. Wang, S. Chen, D. Chen, Spontaneous transition of a water droplet from the Wenzel state to the Cassie state: a molecular dynamics simulation study, Phys. Chem. Chem. Phys. 17 (2015) 30533.
[41] D.C. Rapaport, The Art of Molecular Dynamics Simulation, 2nd ed., Cambridge University Press, Cambridge, 2004.
[42] D. Niu, G.H. Tang, The effect of surface wettability on water vapor condensation in nanoscale, Sci. Rep. 6 (2016) 19192.
[43] A. Hens, R. Agarwal, G. Biswas, Nanoscale study of boiling and evaporation in a liquid Ar film on a Pt heater using molecular dynamics simulation, Int. J. Heat and Mass Transfer 71 (2014) 303–312.
[44] R.L. Davidchack, R. Handel, M.V. Tretyako, Langevin thermostat for rigid body dynamics, J. Chem. Phys. 130 (2009) 234101.
[45] B. Coasne, A. Galarneau, F. Di Renzo, R.J.M. Pellenq, Molecular Simulation of Nitrogen Adsorption in Nanoporous Silica, Langmuir 26 (13) (2010) 10872–10881.
[46] J.J. Potoff, J. Siepmann, Vapor–liquid equilibria of mixtures containing alkanes, carbon dioxide, and nitrogen, I. AIChE J. 47 (2001) 1676.
[47] J. Chen, J.-G. Mi, K.-Y. Chan, Comparison of different mixing rules for prediction of density and residual internal energy of binary and ternary Lennard–Jones mixtures, Fluid Phase Equilib. 178 (2001) 87–95.
[48] J. Vrabec, J. Stoll, H. Hasse, Molecular models of unlike interactions in fluid mixtures, Journal of Molecular Simulations 31 (4) (2005) 221.